

## CONTACT FORCE MODELS IN INELASTIC COLLISIONS

Sharen J. CUMMINS<sup>1\*</sup>, Colin Thornton<sup>2</sup> and Paul W. CLEARY<sup>1</sup>

<sup>1</sup> CSIRO Mathematics, Informatics and Statistics, Clayton, Victoria 3169, AUSTRALIA

<sup>2</sup> School of Chemical Engineering, University of Birmingham, Edgbaston, Birmingham, B15 2TT, U.K

\*Corresponding author, E-mail address: sharen.cummins@csiro.au

### ABSTRACT

The Discrete Element Method (DEM) has become a valuable technique in modelling various industrial processes involving granular flows. There are a number of contact force models implemented in DEM that incorporate viscous or plastic dissipation but their validation is a difficult process given their performance is likely problem dependent. In this context, we examine the accuracy of two DEM viscous dissipation models (where the energy is dissipated through a dashpot mechanism) in simulating a simple inelastic oblique impact. We compare the rebound kinematics at various impact angles for a wide range of normal coefficients of restitution for two types of dashpot models against previously validated plastic dissipation models. We discuss two important results. The first is that for high coefficients of restitution both dashpot models behave similarly and compare well to plastic dissipation models. However as the coefficient of restitution decreases (and the energy dissipation increases) both dashpot models produce increasingly damped tangential forces and velocities. This is entirely different behaviour to the validated plastic dissipation models which show increasingly oscillatory tangential forces and velocities as the coefficient of restitution decreases. The final key result is the appropriate choice of the damping coefficient in the viscous dissipation models to ensure the normal coefficient of restitution is correctly reproduced.

### INTRODUCTION

The Discrete Element Method (DEM), originally developed by Cundall and Strack (1979) for quasi-static deformation of compact particle systems is now used for a wide variety of problems ranging from highly collisional rapid granular flows to quasi-static deformation problems with enduring contacts, see for example Thornton (2009). The particle-particle interactions depend on how the contact normal and tangential forces are calculated, i.e the choice of contact force model. There are a number of different contact force models that have been implemented in DEM simulations, all of which incorporate some form of viscous or plastic energy dissipation. However, it is currently unclear what significance the choice of contact force model has on the resulting flow or its properties. Indeed the choice likely depends on whether the problem is highly collisional and/or has enduring contacts. So the validation of DEM contact models is challenging but worthwhile given the importance of DEM in modelling industrial processes. As part of this validation process we have recently completed a study comparing the performance of various contact models for a simple

problem of a sphere impacting obliquely with a target wall, see Thornton et. al (2012). We studied normal and tangential contact force models that can be categorised as either viscous dissipation or plastic dissipation models for a broad range of normal coefficient of restitution. It was found that existing experimental evidence and theoretical models supported the plastic dissipation model behaviour but did not support the viscous dissipation behaviour. The aim of this paper then is to expand further on the limitations of the viscous dissipation models. Specifically we will show how and why the behaviour of the viscous models diverges from the plastic models as the normal coefficient of restitution,  $e_n$  reduces. We will also discuss the choice of dashpot coefficient in these viscous models in order to reproduce the normal coefficient of restitution correctly.

### DESCRIPTION OF CONTACT FORCE MODELS

The most common contact force model is the linear spring-dashpot (LS+D) model introduced by Walton (1983). LS+D models are widely used as they are robust and easy to implement. Non-linear variations of the LS+D model have also been implemented e.g. Tsuji et al. (1992). These dashpot models dissipate energy through viscous means; therefore we will label them viscous dissipation models. Other contact force models, e.g. Stronge (1994) and Thornton (1997), dissipate energy plastically by using different loading and unloading spring stiffnesses. We will call these interaction models plastic dissipation models. In the following sections we describe the viscous dissipation models to be examined and compare their performance to a validated plastic dissipation model.

#### Viscous Dissipation Models

In the following sections we present a linear spring dashpot and a non-linear spring dashpot model.

#### Linear Spring Dashpot Model (LS+D)

In the linear spring dashpot model (LS+D) the normal and tangential forces are calculated using the following equations below,

$$\begin{aligned} F_n &= k_n \alpha + 2\gamma \sqrt{mk_n} v_n \\ F_{te}^n &= F_{te}^{n-1} + k_t \Delta \delta \\ F_t &= F_{te}^n + 2\gamma \sqrt{mk_t} v_t \quad \text{if } F_t \geq \mu F_n \text{ then } F_t = \mu F_n \quad (1) \end{aligned}$$

where  $F_n$  is the normal force,  $F_t$  is the tangential force,  $F_{te}$  is the elastic component of the tangential force,  $\alpha$  is the overlap,  $m$  is the mass,  $k_n$  is the normal spring stiffness,  $v_n$

is the normal surface velocity and  $v_t$  is the tangential surface velocity. The dashpot coefficient  $\gamma$  depends on  $e_n$  and is given by Eq. (6) or Eq. (7). The tangential force is calculated using the relative tangential displacement increment  $\Delta\delta$  at timestep  $n$  with tangential spring stiffness

$$k_t = \kappa k_n$$

where  $\kappa$  is a material quantity dependent on Poisson's ratio  $\nu$

$$\kappa = \frac{2(1-\nu)}{(2-\nu)}$$

The tangential force is limited by Coulomb friction where  $\mu$  is the friction coefficient.

#### Hertz Mindlin Spring Dashpot Model (HM+D)

A non-linear spring-dashpot model can be implemented in which the normal spring is Hertzian and the tangential spring is provided by the 'no slip' theory of Mindlin (1949). This model is referred to as the HM+D model. The normal and tangential contact forces are calculated using

$$\begin{aligned} F_n &= \frac{4}{3} E^* R^{1/2} \alpha^{3/2} + 2\gamma \sqrt{mk_n} v_n \\ F_{te}^n &= F_{te}^{n-1} + k_t^n \Delta\delta \quad \text{for } \Delta F_n \geq 0 \\ F_{te}^n &= F_{te}^{n-1} \left( \frac{k_t^n}{k_t^{n-1}} \right) + k_t^n \Delta\delta \quad \text{for } \Delta F_n < 0 \\ F_t &= F_{te}^n + 2\gamma \sqrt{mk_t} v_t \quad \text{if } F_t \geq \mu F_n \text{ then } F_t = \mu F_n \quad (2) \end{aligned}$$

where the spring stiffnesses now depend on overlap  $\alpha$

$$k_n = 2E^* \sqrt{R\alpha} \quad \text{and} \quad k_t = 8G^* \sqrt{R\alpha}$$

and  $E^*$  and  $G^*$  depend on Young's modulus  $E$ , shear modulus  $G$  and  $\nu$

$$E^* = \frac{E}{2(1-\nu^2)} \quad G^* = \frac{G}{2(2-\nu)} \quad \text{and} \quad G = \frac{E}{2(1+\nu)}$$

#### The PLS(B) Plastic Dissipation Model

We compare the viscous models against the PLS(B) plastic dissipation model introduced in Thornton et. al (2012). This plastic dissipation model was shown to compare well against the validated theoretical model of Thornton (1997). The PLS(B) model incorporates dissipation in both the loading and unloading phases by adjusting the normal spring stiffness in loading ( $k_1$ ) and unloading ( $k_2$ ) with  $e_n$ . The tangential spring stiffness in this model is defined as the normal unloading spring stiffness  $k_2$  multiplied by  $\kappa$ ,

$$\begin{aligned} F_n &= k_1 \alpha = e_n k \alpha \quad \text{for } \Delta F_n \geq 0 \\ F_n &= k_2 (\alpha - \alpha_0) = \frac{k}{e_n} (\alpha - \alpha_0) \quad \text{for } \Delta F_n < 0 \\ F_t^n &= F_t^{n-1} + \kappa k_2 \Delta\delta \quad \text{if } F_t \geq \mu F_n \text{ then } F_t = \mu F_n \quad (3) \end{aligned}$$

## PROBLEM DESCRIPTION

An inelastic collision between a single spherical particle and a planar target wall is examined at different impact angles. The sphere approaches the wall without rotation, adhesive or gravitational forces as described in Thornton et.al (2012) and shown in Figure 1.

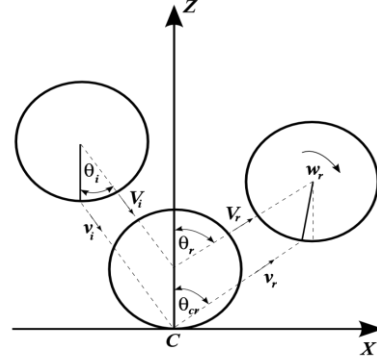


Figure 1: Schematic diagram of the impact geometry.

Figure 1 illustrates diagrammatically a typical oblique impact of a sphere with a target wall. The sphere approaches the wall with an initial translational velocity  $V_i$  at an impact angle  $\theta_i$ . After interaction with the wall the sphere rebounds at an angle  $\theta_r$  with a rebound translational velocity  $V_r$  and a rebound angular velocity  $\omega_r$ .  $V_i$  and  $V_r$  are the velocities of the sphere centre. The corresponding surface velocities at the contact are denoted by  $v_i$  and  $v_r$ .

We examine impact angles only in the range  $0 \leq \theta_i \leq 45^\circ$  as sliding occurs throughout the entire impact for  $\theta_i > 45^\circ$  (and therefore the results are identical for all models). To simplify comparisons between the different contact force models, we consider a constant normal impact velocity  $V_{ni} = 5$  m/s and simulate impacts at angles  $\theta_i = 1, 5, 10, 15, 20, 25, 30, 35, 40$  and  $45$  degrees. For all models we consider an elastic sphere of radius  $R = 25$  mm, density  $\rho = 2650$  kg/m<sup>3</sup> and mass  $m = 0.1734$  kg. The interface friction is  $\mu = 0.1$ ,  $E = 70$  GPa and  $\nu = 0.3$ . Following Thornton et. al. (2011) we characterise the rebound kinematics by the normalised impact angle  $\Theta$  and the normalised rebound tangential surface velocity  $\Psi$

$$\Theta = \frac{2 \tan \theta_i}{(1 + e_n) \mu} \quad \Psi = \frac{2v_{tr}}{(1 + e_n) \mu V_{ni}}$$

## RESULTS

The rebound kinematics for the viscous models previously described are presented and discussed as  $e_n$  decreases from 0.9 to 0.25. Where appropriate the tangential force evolution curves are also presented for further insight. For the simple impact problem studied we compare our results against the partially latching spring model PLS(B) introduced in Thornton et. al (2012).

#### Viscous Model Behaviour As Coefficient of Restitution Reduces

In Thornton et. al. (2012) we presented results for the rebound kinematics for both the viscous models (LS+D, HM+D) and compared them against various plastic

dissipation models including PLS(B). Figures 2, 3 and 4 show the rebound kinematics for the LS+D, HM+D and PLS(B) models respectively and are reproduced here from Thornton et. al. (2012) to aid in further analysis and discussion. Interpretation of these figures is also discussed in Thornton et. al. (2012).

As can be seen from Figures 2 and 3 both viscous models behave similarly as  $e_n$  reduces. So the choice of viscous model has only a minor effect on the rebound kinematics. The key point we want to expand on in this paper is in understanding the difference in behaviour between the viscous models and the plastic models as  $e_n$  reduces, particularly for  $e_n < 0.5$ . To do this we need to consider both the rebound kinematics and the tangential force evolution curves. These differences are noted by first examining the rebound kinematics results for  $e_n = 0.25$  in Figures 2, 3 and 4. Figure 4 shows that for  $e_n = 0.25$  an additional oscillation in  $v_{tr}$  occurs in the PLS(B) results which is not observed in either the LS+D or HM+D results in Figures 2 and 3. In addition at low  $e_n$  values the viscous dissipation models produce a moderately negative  $v_{tr}$  that varies slowly with impact angle. In contrast, the PLS(B) model exhibits an oscillatory behaviour in  $v_{tr}$  with positive and negative values larger in magnitude. We noted too in the course of our study that as  $e_n$  reduced further, more oscillations in  $v_{tr}$  occur for the PLS(B) model while for the viscous models further damping of  $v_{tr}$  occurs.

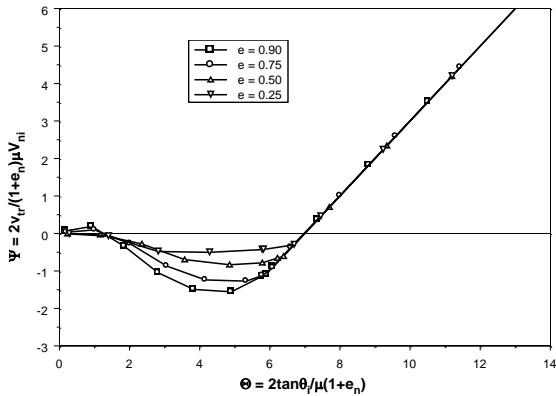


**Figure 2:** Normalised rebound tangential surface velocity  $\Psi$  vs normalised impact angle  $\Theta$  for the LS+D model.

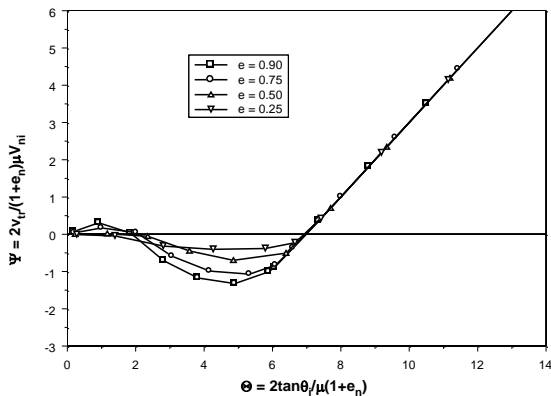


**Figure 3:** Normalised rebound tangential surface velocity  $\Psi$  vs normalised impact angle  $\Theta$  for the HM+D model

To explore the differences in behaviour between the viscous and plastic dissipation models as  $e_n$  reduces it is useful to examine the tangential force evolution with time for both viscous models and compare these evolution curves to the PLS(B) model. The tangential force  $F_t$  at the end of the collision (assuming no sliding occurs) is directly related to the rebound tangential velocity. So it is relevant to examine these evolution curves towards the end of the collision particularly as  $e_n$  reduces.

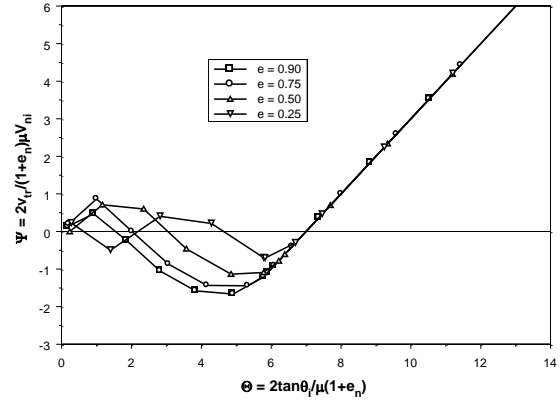


**Figure 4:** Normalised rebound tangential surface velocity  $\Psi$  vs normalised impact angle  $\Theta$  for the PLS(B) model.

Figures 5 and 6 show the tangential force evolution curves for the LS+D model at  $e_n = 0.5$  and  $e_n = 0.25$  respectively. Figures 7 and 8 show these curves for the HM+D model. For the two viscous models the behaviour is generally similar. As  $e_n$  reduces the initial tangential force at the start of the contact increases and then decays away. This large initial tangential force is explained easily by examining Eqs. (1) or (2). As  $e_n$  reduces the dashpot coefficient  $\gamma$  increases (as discussed in the next section) so the initial tangential force  $F_t$  also increases. It also occurs sooner in the contact. In fact for the LS+D  $e_n = 0.25$  results the maximum tangential force occurs at the start of the contact (when the velocity is largest and the damping term in Eq. (1) most dominant). Both viscous models show a significant decay in the tangential force towards the end of the impact before sliding occurs as impact angle and  $e_n$  reduce. The LS+D and HM+D models mimic a highly damped mass-spring system at low  $e_n$  where the damping component of  $F_t$  dominates the elastic component  $F_{te}$  in Eq. (1) or Eq. (2), i.e

$$F_t \approx 2\gamma\sqrt{mk_t}v_t \quad (4)$$

Focusing now on the LS+D results, we note the variation in  $F_t$  in Figures 5 and 6 towards the end of the collision (just before sliding occurs) with impact angle and  $e_n$  is directly correlated with the variation in rebound tangential velocity  $v_{tr}$  in Figure 2. This correlation is explained by Eq. (4), i.e the tangential force towards the end of the impact is closely related to the tangential velocity at the end of the impact  $v_{tr}$

$$F_t \approx 2\gamma\sqrt{mk_t}v_{tr}$$

because of the dominant dashpot component in the tangential force equation. This domination increases as  $e_n$

reduces. A similar correlation is noted for the HM+D model by examining Figures 7 and 8 and Figure 3.

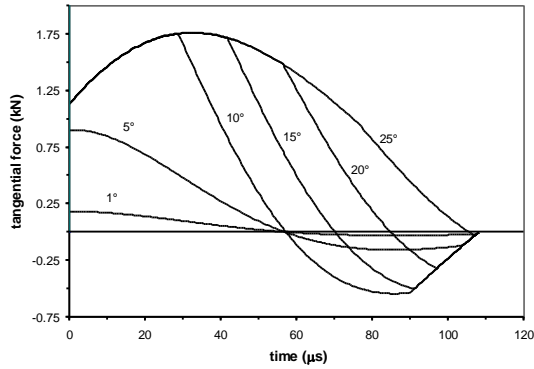


**Figure 5:** Tangential force vs time for the LS+D model,  $e_n = 0.5$  for various impact angles  $\theta_1$ .

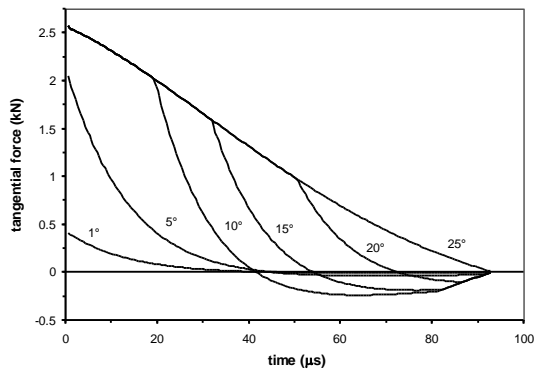


**Figure 6:** Tangential force vs time for the LS+D model,  $e_n = 0.25$  for various impact angles  $\theta_1$ .

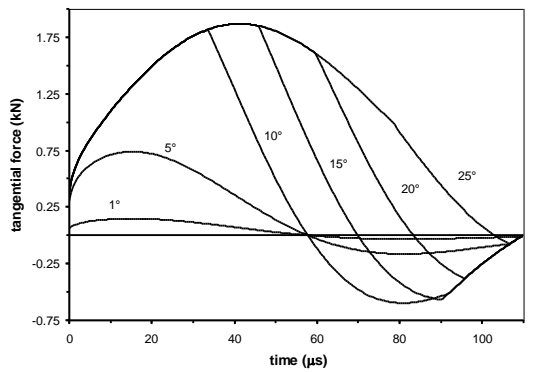


**Figure 7:** Tangential force vs time for the HM+D model,  $e_n = 0.5$  for various impact angles  $\theta_1$ .

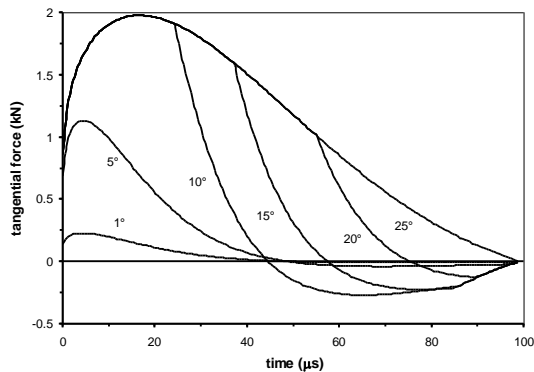


**Figure 8:** Tangential force vs time for the HM+D model,  $e_n = 0.25$  for various impact angles  $\theta_1$ .

In contrast, Figures 9 and 10 show the tangential force evolution curves for the PLS(B) model at  $e_n = 0.5$  and  $e_n = 0.25$  respectively. The tangential force behaviour differs remarkably from that observed in the LS+D and HM+D models. The PLS(B) results in Figure 9 show that using  $e_n = 0.5$  leads to oscillatory tangential forces whose frequency increases with decreasing impact angle. Reducing  $e_n$  further leads to increasingly oscillatory tangential forces for the PLS(B) model. There is also very little dissipation as  $e_n$  reduces, unlike the viscous models. The reason for this increasing oscillation as  $e_n$  reduces is explained by considering the ratio of the tangential spring stiffness to the normal loading spring stiffness for the PLS(B) model. From Eq. (3) this ratio is

$$\kappa_1 = \frac{k_t}{k_1} = \frac{\kappa_2}{k_1} = \frac{\kappa}{e_n^2} \quad (5)$$

which increases as  $e_n$  reduces. That is, in the PLS(B) model the tangential spring stiffness increases relative to the normal loading stiffness as  $e_n$  reduces. This results in a stiffer system in the tangential direction leading to the increased tangential force oscillations. In the viscous models this stiffness ratio  $\kappa l$  does not change as  $e_n$  changes (since a constant normal stiffness  $k$  is used in the viscous models). In addition the dashpot term dominates the tangential force as  $e_n$  reduces.

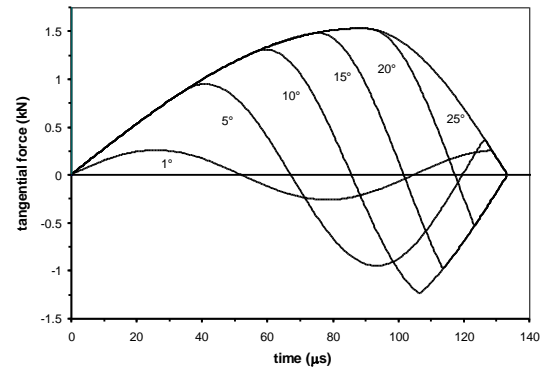


**Figure 9:** Tangential force vs time for the PLS(B) model,  $e_n = 0.5$  for various impact angles  $\theta_1$ .

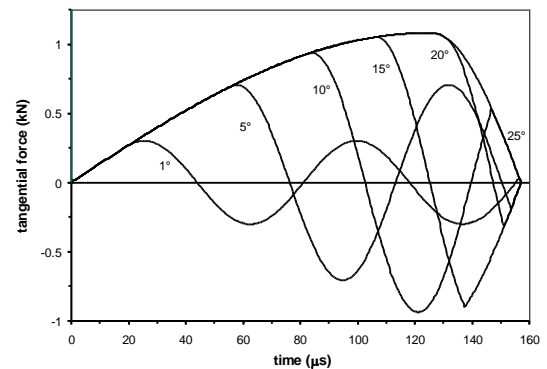


**Figure 10:** Tangential force vs time for the PLS(B) model,  $e_n = 0.25$  for various impact angles  $\theta_1$ .

It was noted in Thornton et al. (2012) that the plastic dissipation models are well supported by experimental evidence. The authors are not aware of any experimental evidence (which albeit is focussed on elastoplastic materials) to support the force evolution exhibited by the viscous dissipation models. A possible exception to this is Behera et al. (2005) who studied fragmentation and damage of an agglomerated disc impacting a plate. It may be that the viscous dissipation models are more suited to friable materials that fracture at the contact.

### The Correct Dashpot Coefficient In the Viscous Models

In studying the sensitivity of the rebound characteristics to  $e_n$  for the LS+D model we initially used the traditional dashpot coefficient equation from Schafer (1996),

$$\gamma = \frac{-\ln e_n}{\sqrt{\pi^2 + \ln^2 e_n}} \quad (6)$$

Eq. (6) provides the value for  $\gamma$  in Eq. (1) in order to produce a desired  $e_n$  in the collision. In reducing  $e_n$  (increasing  $\gamma$ ) we found an increasing discrepancy between the measured and desired  $e_n$  values. Figure 11 shows the measured vs desired  $e_n$  values for LS+D simulations that were run with impact angle  $\theta_i = 0^\circ$ . (The measured  $e_n$  values were calculated by taking the ratio of the normal rebound and normal impact velocities). As the desired  $e_n$  value reduces the difference between the measured and desired  $e_n$  values increases. In fact we found we were never able to produce a measured  $e_n < 0.15$  when the traditional Eq. (6) was used for the dashpot coefficient in the LS+D model.

Schafer (1996) originally derived Eq. (6) for the LS+D model by calculating the velocity in a damped harmonic oscillator at the time when the displacement returns to zero. This velocity along with the known initial velocity was then used to derive the expression for  $\gamma$  as a function of  $e_n$  in Eq. (6). Schwager and Poschel (2007), however, highlighted that DEM interactions finish when the force returns to zero, not when the displacement returns to zero (unless adhesion is modelled). The velocity used in the  $e_n$  derivation should therefore be measured when the force returns to zero, not when the displacement returns to zero.

To highlight this distinction Figure 12 shows the displacement, velocity and force vs contact time for  $e_n = 0.5$  for  $\theta_i = 0^\circ$  using the LS+D model. The time when the displacement first returns to zero is denoted as  $t_1$  and the time when the force returns to zero is denoted as  $t_2$ . Figure 12 shows the rebound velocities at times  $t_1$  and  $t_2$  differ and therefore the  $e_n$  values differ. The limitation with Eq. (6) is that it is derived using the velocity at time  $t_1$  (when the displacement returns to zero). However for DEM simulations (that do not model adhesion), the velocity at time  $t_2$  should be used (when the force returns to zero).

For the LS+D model, Schwager and Poschel (2007) derived the following solution for  $e_n$  as a function of  $\gamma$  when the velocity is calculated at the time when the force returns to zero (i.e at time  $t_2$  in Figure 12)

$$\begin{aligned} \ln e_n &= -\frac{\gamma}{\sqrt{1-\gamma^2}} \left[ \pi - \arctan \left( \frac{2\gamma\sqrt{1-\gamma^2}}{2\gamma^2-1} \right) \right] & \text{for } \gamma \leq \frac{1}{\sqrt{2}} \\ \ln e_n &= -\frac{\gamma}{\sqrt{1-\gamma^2}} \arctan \left( \frac{2\gamma\sqrt{1-\gamma^2}}{2\gamma^2-1} \right) & \text{for } 1 \geq \gamma \geq \frac{1}{\sqrt{2}} \\ \ln e_n &= -\frac{\gamma}{\sqrt{\gamma^2-1}} \ln \left[ \frac{\left( \frac{\gamma}{\sqrt{\gamma^2-1}} \right) + 1}{\left( \frac{\gamma}{\sqrt{\gamma^2-1}} \right) - 1} \right] & \text{for } \gamma \geq 1 \end{aligned} \quad (7)$$

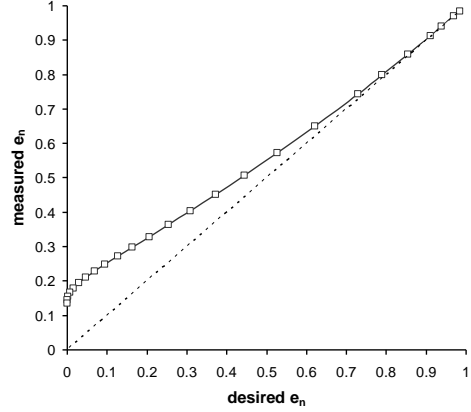


Figure 11: Measured versus desired  $e_n$  values using LS+D

Figure 13 shows the comparison between Eq. (7) for  $\gamma$  labelled as ‘Poschel’ in the figure versus the traditional Eq. (6) labelled as ‘Schafer’ in the figure. As  $e_n$  reduces the differences in  $\gamma$  increase with Eq. (7) providing a much larger  $\gamma$  as  $e_n$  reduces. The traditional Eq. (6) producing  $\gamma$  values no greater than 1.0. We note the measured  $e_n$  values in Figure 11 for the LS+D simulations are reproduced closely by Eq. (7).

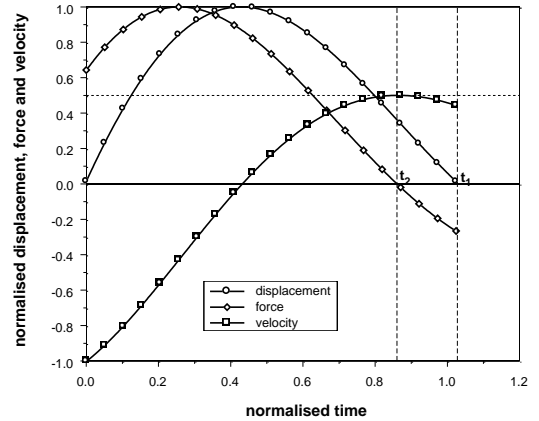


Figure 12: Displacement, velocity and force evolution curves using LS+D with  $e_n = 0.5$ .

While Eq. (7) is the correct equation for  $\gamma$  in the LS+D model, it is difficult to implement in a DEM code which typically requires  $e_n$  as the inputted parameter rather than  $\gamma$  (since  $e_n$  is a known material quantity). We therefore used curve fitting techniques on Eq. (7) to formulate the following expression for  $\gamma$  as a function of  $e_n$

$$\gamma = e_n(1 - e_n)^2 \xi$$

$$\xi = [h_1 + \beta(h_2 + \beta(h_3 + \beta(h_4 + \beta(h_5 + \beta(h_6 + \beta(h_7 + \beta(h_8 + \beta(h_9 + \beta(h_{10})))))))))))]$$

$$\beta = e_n - 0.5 \quad (8)$$

where the coefficients  $h_i$  are tabulated in Table 1. Figure 13 also shows this fitted curve.

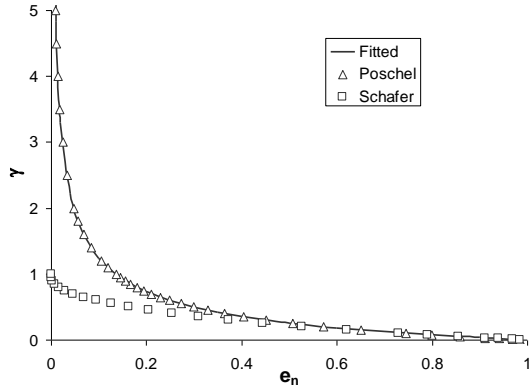


**Figure 12:** Dashpot coefficient  $\gamma$  vs  $e_n$  using Eq. (6) (Schafer), Eq. (7) (Poschel) and Eq. (8) (Fitted).

It may be possible to derive an analytic expression for  $\gamma$  in the HM+D model but this is currently beyond the scope of this work. Schwager and Poschel (2008) formulated an expression for  $e_n$  in terms of  $\gamma$  for a similar system to the HM+D model presented in this paper. This expression was also dependant on the impact velocity.

$i$	$h_i$
1	0.2446517
2	-0.5433478
3	0.9280126
4	-1.5897793
5	1.2102729
6	3.3815393
7	6.3814014
8	-34.482428
9	25.672467
10	94.396267

**Table 1:** Coefficients  $h_i$  used in Eq. (8) for  $\gamma$

## CONCLUSION

We have explored limitations of the viscous dissipation models as the energy dissipation increases by examining how the rebound kinematics and collisional force evolution curves vary as  $e_n$  reduces. For  $e_n \leq 0.5$  the viscous models produce increasingly smaller tangential surface velocities due to the dominant dashpot term in the tangential force equation. This is in contrast to validated plastic models which produce increasingly oscillatory behaviour in the tangential surface velocities as  $e_n$  reduces. Existing experimental evidence and theoretical models support the plastic behaviour but do not support the viscous behaviour. In addition, the traditional equation for

the dashpot coefficient originally proposed by Schafer (1996) for the LS+D model does not reproduce the correct  $e_n$  values for non-adhesive interactions. The dashpot coefficient equation provided by Schwager and Poschel (2007) has been demonstrated to correctly reproduce the  $e_n$  values and a more easily implementable form of this equation has been formulated.

We have limited our analysis to a spherical particle impacting against a rigid planar wall for brevity. We expect similar differences between the models to carry over for cases where both bodies are deformable (such as two particles colliding). Further details related to this area can be found in Wu et. al (2009) where impacts between deformable bodies was examined. While validation does not exist for non-spherical particle impact we would also expect the trends discussed in this paper to be similar for non-spherical particle impact. These trends are dependant on the choice of contact force model which, in turn, is independent of particle shape. This is an interesting area for further exploration with the primary challenge being validation.

## REFERENCES

- BEHERA, B., KUN, F., MCNAMARA, S., HERMANN, H.J., (2005), "Fragmentation of a circular disk by impact on a frictionless plate", *Journal of Physics: Condensed Matter*, **17**, S2349-S2456
- CUNDALL, P.A. and STRACK, O.D.L., (1979), "A discrete numerical model for granular assemblies", *Geotechnique*, **29**, 47-65
- THORNTON, C., (2009), "Special Issue on the 4<sup>th</sup>. Int. Conf. on Discrete Element Methods", *Powder Technol.*, **193**, 216-336
- THORNTON, C., CUMMINS, S. J. and CLEARY, P.W., (2012), "An investigation of the comparative behaviour of alternative contact force models during inelastic collisions", *Powder Technol.*, **233**, 30-46
- WALTON, O.R., (1983), "Application of molecular dynamics to macroscopic particles", *Int. J. Eng. Sci.*, **22**, 1097-1107
- TSUJI, Y., TANAKA, T. and ISHIDA, T., (1992), "Lagrangian numerical simulation of plug flow of cohesionless particles in a horizontal pipe", *Powder Technol.*, **71**, 239-245
- THORNTON, C., (1997), "Coefficient of restitution for collinear collisions of elastic-perfectly plastic spheres", *Trans. ASME J. Appl. Mech.*, **64**, 383-386.
- STRONGE, W.J., (1994), "Planar impact of rough compliant bodies", *Int. J. Impact Engineering*, **15**, 435-450
- MINDLIN, R.D., (1949), "Compliance of elastic bodies in contact", *Trans. ASME J. Appl. Mech.*, **16**, 259-268.
- SCHAFFER, J., DIPPEL, S. and WOLF, D.E., (1996), "Force schemes in simulations of granular materials", *Journal de Physique I*, **6**, 5-20
- SCHWAGER, T. and POSCHEL, T., (2007), "Coefficient of restitution and linear-dashpot model revisited", *Granular Matter*, **9**, 465-469
- SCHWAGER, T. and POSCHEL, T., (2008), "Coefficient of restitution for viscoelastic spheres: The effect of delayed recovery", *Phys. Rev. E*, **78**, 051304
- WU, C.Y., THORNTON, C. and LI, L.-Y., (2009), "A semi-analytical model for oblique impacts of elastoplastic spheres", *Proceedings of Royal Society of London A* **465**, 937-960